JOURNAL INDIAN ASSOCIATION OF SEDIMENTOLOGISTS ISSN NO 2582 – 2020
Vol. 43, Issue I, 2026, pp. 79 – 98

Sedimentological studies of the Katesar Member (Late Jurassic), Jhuran Formation, Kachchh basin: An example of transition from Delta Front to Delta Plain settings.

Poonam R. Mangtani* **and A.V. Joshi**
Department of Geology, Faculty of Science, The Maharaja Sayajirao University of Baroda, Vadodara-390002, Gujarat, India.

A R T I C L E I N F O

KEYWORDS:

Jhuran Formation;

Katesar Member;

Sedimentology;

Delta Plain;

A B S T R A C T

The Kachchh Basin of western India preserves a thick Mesozoic succession deposited in a pericratonic rift setting along the northern margin of the Indian plate. Within this succession, the Late Jurassic Jhuran Formation, comprising the Lower, Middle, Upper and Katesar Members, records extensive siliciclastic sedimentation. The present study aims to evaluate the nature of sedimentation and reconstruct the depositional environment of the Katesar Member using facies analysis, petrography, heavy mineral assemblages, bulk mineralogy and geochemical proxies. The facies analysis of the Katesar Member reveals the presence of hummocky cross-stratified sandstones, bioturbated ferruginous sandstones, thin-bedded sandstone-siltstone alternations and gypsiferous shale, indicating deposition in a wave-dominated delta-front setting under episodic storm influence. Heavy mineral assemblages and bulk mineralogical data suggest sediment derivation predominantly from felsic source rocks with evidence of recycling. Geochemical analyses of major, minor and trace elements indicate a provenance consistent with a stable continental setting, ranging from craton interior to passive margin conditions and suggest moderate to strong chemical weathering. The integration of sedimentological and geochemical proxies enables a robust reconstruction of sediment dispersal pathways, provenance, and depositional dynamics of the Katesar Member. The results indicate a progressive transition from delta-front to delta-plain environments, marked by an upward shift from storm-influenced, hummocky cross-stratified sandstones to planar- and ripple-laminated facies, a decline in marine faunal elements, increased development of heterolithic units, and the occurrence of ferruginous and gypsiferous horizons reflecting subaerial exposure. These signatures collectively constrain the progradational evolution of a deltaic system in the Kachchh Basin during the Late Jurassic.

INTRODUCTION

The Mesozoic succession of the Kachchh Basin of western India represents one of the most complete and well-exposed records of rift-related sedimentation along the northwestern margin of the Indian plate (Biswas, 1982, 1993; Fürsich and Pandey, 2003). The basin developed as a pericratonic rift with episodic marine incursions from the Tethys Ocean, resulting in alternating siliciclastic and carbonate deposition (Krishna, 2017). The Mesozoic succession of the Kachchh Basin is classically subdivided into four major lithostratigraphic units- Jhurio, Jumara, Jhuran and Bhuj Formations (Biswas, 1987), which collectively record sedimentation under predominantly marine to marginal-marine conditions, ranging from offshore shelf to deltaic and fluvio-deltaic environments (Biswas, 1993; Fürsich et al., 2001). Among these, the Jhuran Formation (Oxfordian–Tithonian) is a thick siliciclastic unit, broadly interpreted as the product of fluvio-deltaic to shallow marine processes (Bose et al., 1988; Chaudhuri et al., 2018; Desai and Biswas, 2018; Mangtani and Joshi, 2025).

Although previous studies have largely focused on the lithostratigraphy, palaeontology, and sequence stratigraphy of the Jhuran Formation (Biswas, 1991; Fürsich et al., 2001; Arora et al., 2015), the Katesar

Corresponding Author
Email: mangtanipoonam.geology@gmail.com, orcid- id: 0000-0003-2651-7115
DOI: https://doi.org/10.51710/jias.v43iI.460
Received 27 March 2026; Received in revised form 11 May 2026; Accepted 13 May 2026Available online 30 June 2026

Member has received less attention in terms of detailed sedimentology and geochemical proxies, which can also be helpful in unravelling depositional and provenance signatures.

The present study focuses on developing a detailed facies model for the Katesar Member, along with characterizing its heavy mineral assemblages and bulk mineralogy. Geochemical proxies are employed to constrain provenance, palaeoweathering, and tectonic setting, and these datasets are subsequently integrated to reconstruct sedimentation patterns within the Katesar Member of the Jhuran Formation. This integrated approach provides important constraints on the depositional evolution of the Kachchh Basin and offers a representative example of deltaic sedimentation along a rifted continental margin.

GEOLOGY OF THE STUDY AREA

The study area is located in the western part of the Kachchh Basin, between latitudes N 23°46′24.04″ to N 23°46′45″ and longitudes E 68°52′50″ to E 68°56′36″ (Fig. 1). The area is structurally bounded by the Kachchh Mainland Fault (KMF) along its northern margin and is dissected by NE–SW and NW–SE trending transverse faults. The rocks of the Katesar Member are well exposed around the Mundhan dome, Katesar River section, and Guneri dome, comprising ~100 m of sedimentary succession (Mangtani and Joshi, 2024). Stratigraphically, the Katesar Member occupies the uppermost position within the Jhuran Formation in the Mundhan dome, while in the Guneri dome, it occurs at a relatively lower stratigraphic level within the formation. The unit is restricted to the northwestern mainland, with its type section located in a stream south of Sahera near the Katesar Mahadev temple. It comprises a range of lithofacies including gypsiferous shales, hummocky cross-stratified sandstones, bioturbated ferruginous sandstones, thin-bedded sandstone -siltstone alternations, and rippled sandstones, reflecting deposition under variable energy conditions (Table 1).

METHODOLOGY

The methodology employed in this study integrates field-based observations with laboratory analyses. Field investigations involved systematic outcrop documentation, detailed mapping of lithological sections, and correlation of lithounits across the study area. Representative sections of the Katesar Member were measured to record vertical facies variations, sedimentary structures, and stratigraphic relationships.

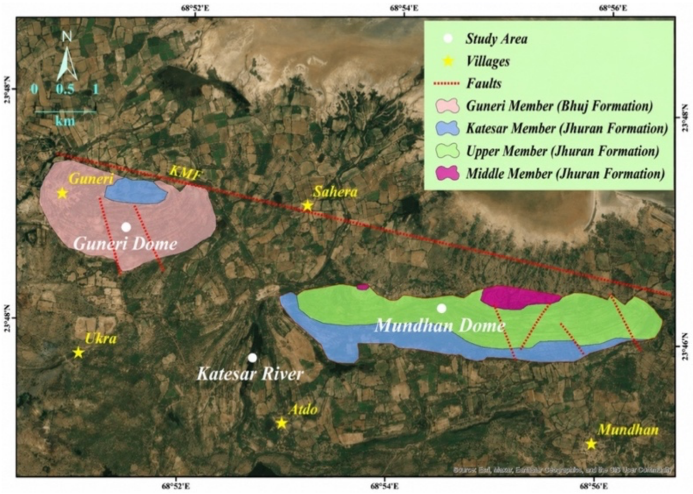

Fig 1. Geological map of the study area

The representative samples from different lithofacies of the Katesar Member were collected for petrographic analysis. Thin sections were prepared and examined under a Leica MC120 HD polarizing microscope. Modal composition of detrital grains was determined using the Gazzi–Dickinson point-counting method (Dickinson, 1970; Ingersoll, 1988), wherein individual sand-sized mineral grains within lithic fragments are counted as discrete mineral phases (Table 2). However, lithic fragments were also recorded where identifiable, allowing classification using Q–F–L parameters and construction of provenance discrimination diagrams. The sandstones were classified following the scheme of Dott (1964) (Fig.12), while fine-grained rocks (including siltstones and shales) were described based on their textural and compositional attributes following established sedimentological criteria (Picard, 1971).

Table 1: Lithofacies of Katesar Member of Jhuran Formation observed in the Mundhan dome, Guneri dome and Katesar river section

Formation	Member	Lithofacies
Jhuran Formation	Katesar Member	11.Fossiliferous Sandstones Facies (FS)
		10. Pebbly Sandstone Facies (PS)
		9. Planar Cross bedded sandstone Facies (PCBS)
		8. Ferruginous Sandstones Facies (FES)
		7. Conglomerate Facies (CO)
		6. Rippled Sandstone Facies (RS)
		5. Thinly Bedded Sandstone Facies (TBSS)
		4. Intercalated Shale-Siltstone Facies (ISHS)
		3. Bioturbated Ferruginous Sandstone Facies (BFS)
		2. Hummocky Cross Stratified Sandstones Facies (HCSS)
		1. Gypsiferous shale Facies (GS)

Heavy mineral analysis was carried out on selected sandstone samples to infer provenance characteristics. The 63–125 µm size fraction was separated and treated with dilute HCl to remove carbonate cement and adhering fines, followed by washing and drying at ~50°C. Heavy minerals were then separated using bromoform (specific gravity ~2.89 g/cm³) through gravity settling techniques (Mange and Maurer, 1992). The separated heavy fraction was washed with distilled water and acetone, dried, and mounted on glass slides for identification under a polarizing microscope.

Table 2: Modal analysis data for different facies of Katesar Member

Sample no.	Facies	Q (%)	F (%)	L (%)	Qm (%)	Qp (%)	Matrix (%)	Cement (%)
KS-1	Gypsiferous Shale (GS)	—	—	—	—	—	—	—
KS-2	Hummocky Cross Stratified Sandstone (HCSS)	92	5	3	80	12	4	8
KS-3	Bioturbated Ferruginous Sandstone (BFS)	88	6	6	75	13	5	7
KS-4	Intercalated Shale–Siltstone (ISHS)	—	—	—	—	—	—	—
KS-5	Thinly Bedded Sandstone (TBSS)	85	5	10	70	15	5	7
KS-6	Rippled Sandstone (RS)	90	7	3	78	12	4	5
KS-7	Conglomerate (CO)	87	5	8	72	15	6	7
KS-8	Ferruginous Sandstone (FES)	92	5	3	80	12	7	8
KS-9	Planar Cross-Bedded Sandstone (PCBS)	88	8	4	74	14	6	10
KS-10	Pebbly Sandstone (PS)	86	5	9	72	14	8	12
KS-11	Fossiliferous Sandstone (FS)	87	5	8	73	14	10	15

The geochemical analyses were carried out to determine the major oxide and trace element composition of representative samples from different lithofacies of the Katesar Member. The samples were pulverized and homogenized to a fine powder (<270 ASTM mesh size) using an agate mortar to avoid contamination. Approximately 20 g of each sample was used for analysis. Major element oxides were determined using X-ray fluorescence (XRF), while trace elements were analysed using inductively coupled plasma mass spectrometry (ICP-MS). The analyses were conducted using an Axios Max Panalytical WD-XRF at the Sophisticated Instrumentation Centre for Applied Research and Testing, Anand, and ICP-MS at the Physical Research Laboratory, Ahmedabad, Gujarat. Loss on Ignition (LOI) was determined by heating pre-weighed powdered samples at ~900–1000°C to estimate weight loss due to volatile components such as bound water, organic matter, and carbonates (Heiri et al., 2001).

From the data obtained from major oxides, different weathering indices such as chemical index of alteration (CIA), chemical index of weathering (CIW), plagioclase index of alteration (PIA), and index of chemical variability (ICV), have been calculated using the following formula.

- CIA = $[Al_2O_3/ (Al_2O_3 + CaO^* + Na_2O + K2O)] \times 100)$ (after Nesbit and Young, 1982);
- CIW = $[Al_2O_3/ (Al_2O_3 + CaO^* + Na_2O)] \times 100$ (after Harnois,1988);
- PIA = $100[(Al_2O_3 – K_2O)/ (Al_2O_3 + CaO + Na_2O- K_2O)]$ (after Fedo et al., 1995); and
- ICV = $((Fe_2O_3 + MnO + MgO + CaO + Na_2O+ K_2O+ TiO_2)/Al_2O_3))$, (after Cox et al., 1995).

To calculate CIA and CIW, CaO* is considered as the amount of CaO incorporated in the silicate fraction of the rock, rather than the carbonate contribution due to the absence of CO_2 value. Thus, to compute CaO* from the silicate fraction, the assumption proposed by Bock et al. (1998) was employed. Based on this, CaO values were accepted only if $CaO<Na_2O$. Thus, when $CaO>Na_2O$, it was presumed that the CaO concentration was the same as that of Na_2O.

The bulk mineralogical composition, including clay and non-clay minerals, was determined using X-ray diffraction (XRD) technique. Finely powdered samples (<270 ASTM mesh size) were analysed using a Rigaku Miniflex diffractometer (Cu Kα radiation) at the Centre for Excellence in Well Logging Technology, ONGC, Vadodara. The obtained diffractograms were interpreted by matching peak positions and intensities with standard reference patterns from the Joint Committee on Powder Diffraction Standards (JCPDS) database.

RESULTS

Lithofacies Analysis

The rocks of the Katesar Member represent the youngest stratigraphic unit of the Jhuran Formation observed in the Mundhan dome. It is restricted to the northwestern part of the mainland, with its designated type section exposed in a stream south of Sahera near the temple of Katesar Mahadev. This member attains a maximum thickness of 55 metres and comprises various facies such as gypsiferous shales, hummocky cross stratified sandstones, bioturbated ferruginous sandstones, intercalated shale-siltstone, thinly bedded sandstone facies, rippled sandstones, conglomerates - ferruginous sandstones, planar cross bedded sandstones, pebbly sandstones and fossiliferous sandstones in stratigraphic order (Fig. 2)

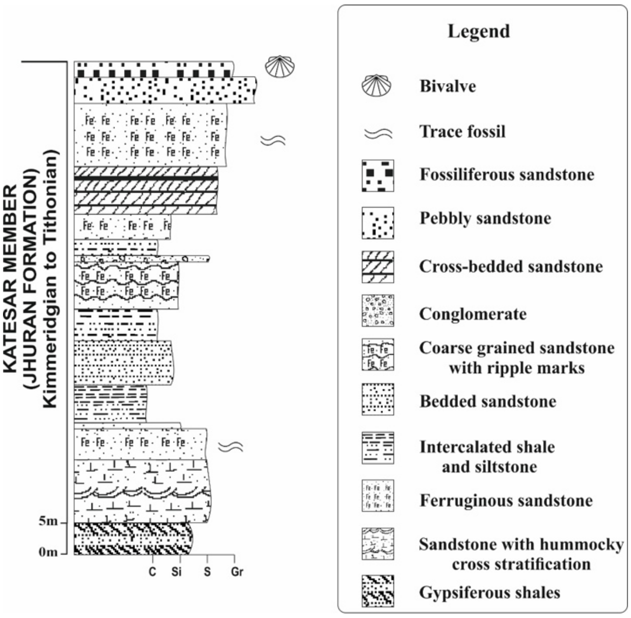

Fig. 2. Composite Litholog showing facies of Katesar Member, Jhuran Formation.

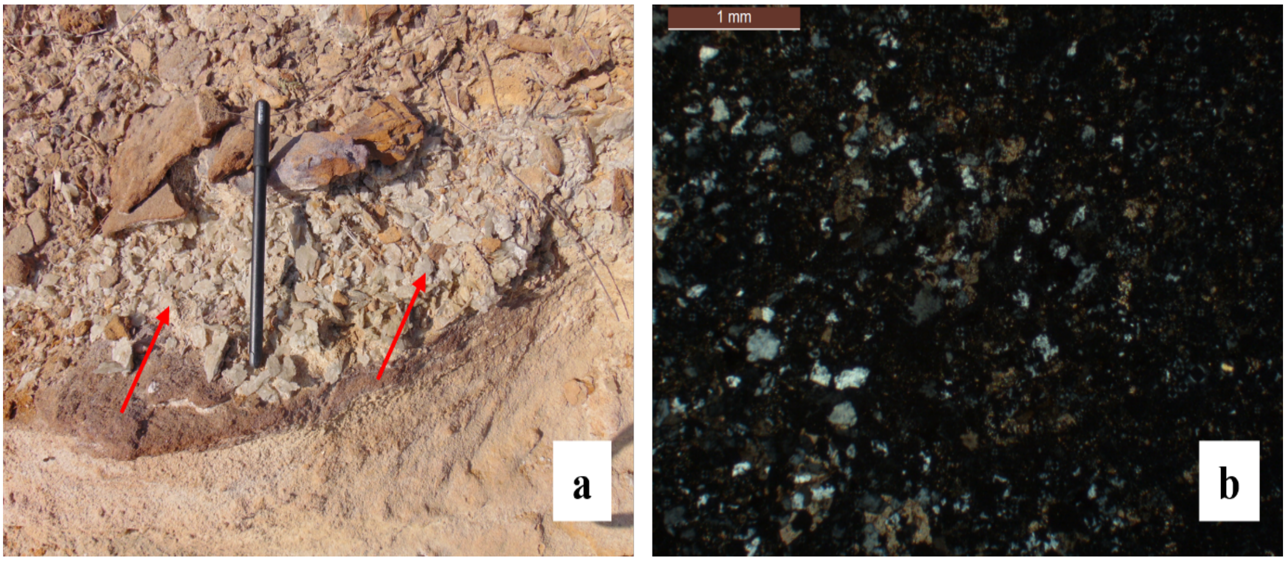

Fig 3. Gypsiferous shales facies: (a) Field photograph showing sandy shale with discontinuous gypsum lenses (scale: pen ~15 cm); (b) Photomicrograph showing presence of monocrystalline quartz and siliceous matrix (XPL); (pen size: 15 cm)

Gypsiferous Shale Facies (GS)

Field Characteristics:

This facies comprises pale brown sandy shales with an exposed thickness ranging from ~0.5 to 3 m, occurring in conformable contact with the underlying units of the Upper Member. The shales are interbedded with fine-grained sandstones and are characterized by the presence of discontinuous gypsum lenses. The gypsum occurs as irregular, lenticular to nodular patches within the shale matrix, likely formed through evaporative concentration and early diagenetic precipitation under restricted conditions (Fig. 3a).

Petrography:

Under the microscope, the sandy shales are composed of angular to sub-angular monocrystalline quartz grains cemented by ferruginous material. The framework grains are fine to medium (0.0125 mm to 0.5 mm), sand sized sub-angular to angular, showing tangential grain to grain contacts with moderate sorting. The framework grains comprise monocrystalline quartz (87–90%), K-feldspars in the form of orthoclase and microcline (5–7%) and mica (muscovite) (1–2%). The grains are embedded in a siliceous matrix and cemented by calcareous material (Fig. 3b).

Hummocky Cross- Stratified Sandstones Facies (HCSS)

Field Characteristics:

This facies comprises pale white to yellow, friable sandstones with individual bed thickness ranging from ~2.5 to 4 m (Fig. 4a). The sandstones are characterized by well-developed hummocky cross-stratification (HCS), expressed as low-angle, undulating laminae forming convex-upward (hummocks) and concave-upward (swales) geometries. These structures are laterally continuous and typically occur within amalgamated sandstone beds, reflecting deposition under combined-flow conditions during storm events. The facies commonly exhibit subtle normal grading and overall fining-upward trends within individual beds, consistent with waning storm energy conditions.

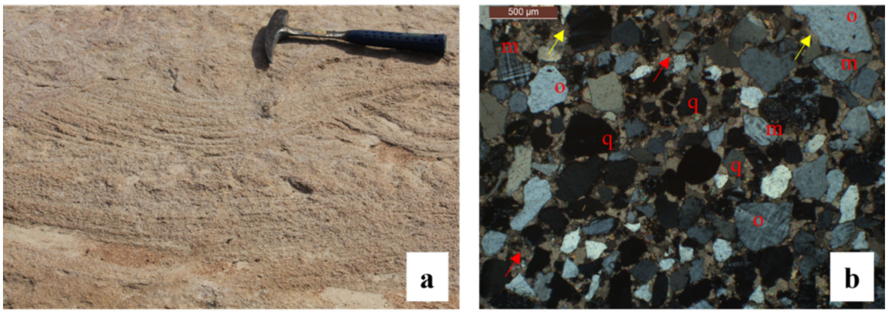

Fig. 4. Hummocky cross stratified sandstones facies: (a) Field photograph showing exposed section with presence of hummocks and swales; (b) Photomicrograph of medium-grained sandstone with angular framework grains of monocrystalline quartz (mq), microcline (m) and orthoclase (o) embedded in siliceous matrix (red arrows), cemented by calcareous cementing material (yellow arrows) (XPL) (hammer size: 30cm)

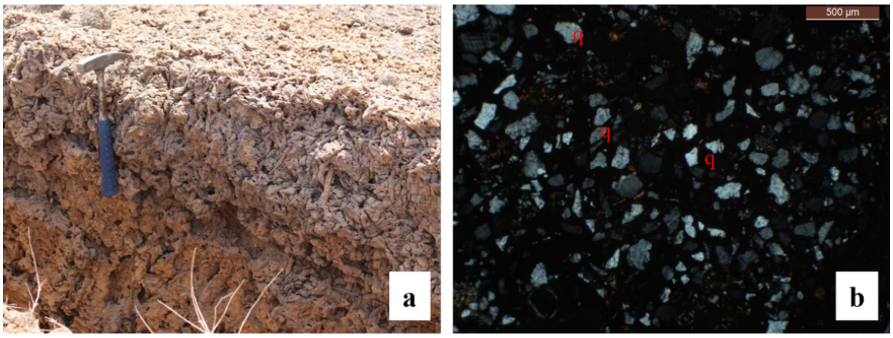

Fig. 5. Bioturbated sandstone facies: **(a)** Field photograph showing exposed section of bioturbated sandstones; **(b)** Photomicrograph of medium-grained sandstone showing presence of quartz (q) however, the texture is disrupted due to organic reworking (XPL) (hammer size: 30cm)

Petrography:

Under the microscope, the sandstones consist of sub-angular to subrounded, medium to coarse (0.5 mm to 1 mm) framework grains showing moderate to poor sorting (Fig. 4b), indicative of a texturally submature nature. The grains show tangential and floating grain to grain contacts and are embedded in a siliceous matrix, cemented by calcareous material. The framework grains constitute monocrystalline and polycrystalline quartz (87–95%), orthoclase (5%) and are indicative of the mineralogically mature nature of these sandstones. Based on the proportion of framework grains and matrix, these sandstones are classified as Quartz Arenites (Dott, 1964).

Bioturbated Ferruginous Sandstone Facies (BFS)

Field Characteristics:

This facies comprises reddish-brown, medium- to coarse-grained sandstones with an exposed thickness of ~3–5 m. The framework grains are predominantly quartz and are cemented by ferruginous material. The sandstones are intensely bioturbated, exhibiting vertical to subvertical cylindrical burrows attributable to *Skolithos*, characterized by straight, unlined to thinly lined tubes with uniform diameter, and branching, horizontally to obliquely oriented burrow networks assignable to *Thalassinoides*, forming interconnected gallery systems (Fig. 5a). Bioturbation has significantly disrupted primary sedimentary structures, resulting in partial to complete homogenization of the original bedding.

Petrography:

Thin section analysis of these sandstones shows medium- to coarse-grained, sub-angular to sub-rounded quartz-dominated framework grains with moderate sorting. The original depositional fabric is largely obliterated due to bioturbation, as reflected by the disrupted and mottled texture observed in thin section (Fig. 5b). The grains are supported by a ferruginous cement, and no well-preserved primary sedimentary structures are evident at the microscopic scale.

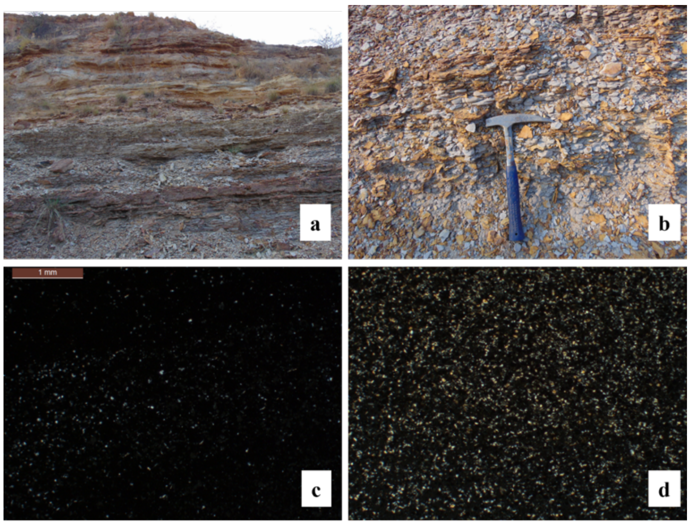

Fig. 6. Intercalated Shale Siltstone Facies: (a) well exposed section showing intercalated sequence of shales and siltstones; (b) Siltstones showing weathered nature and the yellow colouration is due to presence of limonite; (c) Photomicrograph of shale showing very fine detrital grains cemented by ferruginous cement (XPL); (d) Photomicrograph of siltstones showing very fine detrital grains of quartz, cemented by ferruginous material (XPL). (hammer size: 30cm)

Intercalated Shale-Siltstone Facies (ISHS)

Field Characteristics:

This facies attains a maximum exposed thickness of ~18 m and is characterized by alternating beds of siltstone and subordinate shale. The shales are dark grey, fissile, and finely laminated, whereas the siltstones are pale brown to grey, predominantly massive to weakly laminated (Fig. 6 a, b). The rhythmic alternation of fine-grained lithologies reflects deposition under fluctuating low-energy conditions.

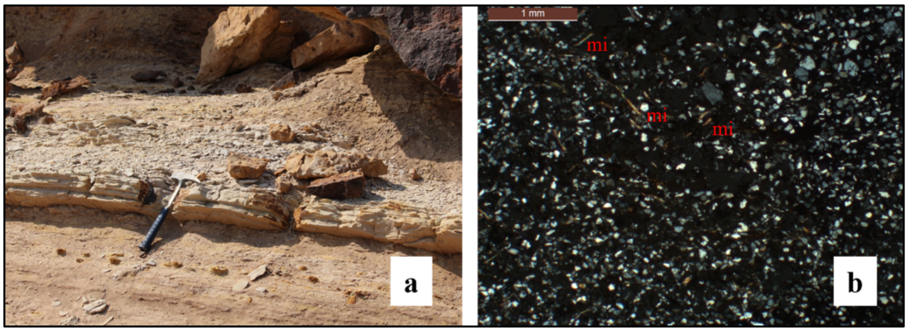

Fig. 7 Thinly bedded sandstone facies: (a) Field photographs showing thinly bedded, laterally continuous sandstone units with planar lamination; (b) Photomicrograph of sandstone with very fine to fine angular grains of monocrystalline quartz (q), orthoclase (o), mica (mi) cemented by ferruginous cementing material (XPL) (hammer size: 30cm)

Petrography:

Petrographic analysis indicates that the shale units are composed predominantly of clay-sized material with minor dispersed fine quartz grains (Fig. 6c). The siltstones consist of angular to sub-angular quartz grains of coarse to medium silt size, with moderate sorting (Fig. 6d). The framework is supported by a fine-grained matrix, and no distinct ferruginous cement is observed in thin section. Based on texture and composition, the shales and siltstones are classified as silty claystone and sandy siltstone, respectively.

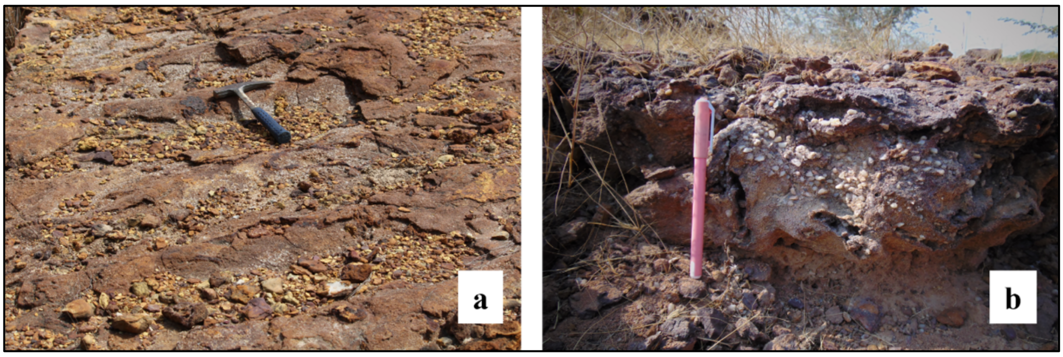

Fig. 8 (a) Field photograph showing well exposed ferruginous sandstones showing the presence of mega ripples; (b) Field photograph showing the conglomerate unit (hammer size: 30 cm; pen size: 15 cm)

Thinly Bedded Sandstones Facies (TBSS)

Field Characteristics:

This facies is characterized by thinly bedded sandstones with an overall thickness of ~5–7 m, exhibiting colours ranging from dark brown to pale yellow. The beds are laterally continuous and display a flaggy nature due to the presence of closely spaced planar lamination and fissility (Fig. 7a). The beds are sub-horizontal to gently inclined and do not exhibit vertical disposition.

Petrography:

Thin section analysis reveals fine- to medium-grained (0.125–0.5 mm), sub-angular to angular moderate to well sorted framework grains, indicating textural sub maturity. Grain to grain contacts are predominantly tangential, with occasional concavo-convex contacts. The detrital composition is dominated by quartz (85–90%), with minor feldspar (orthoclase ~5%) and trace amounts of mica (muscovite and biotite ~2%) (Fig. 7b). The framework grains are supported by a fine matrix and cemented by calcareous material. Based on the relative abundance of framework grains and matrix, these sandstones are classified as Sublithic Arenites (Dott,1964).

Rippled Sandstone Facies (RS)

Field Characteristics:

This facies comprises fine- to medium-grained, reddish-brown sandstones with a thickness ranging from ~0.5 to 2 m. The sandstones are characterized by the presence of well-developed asymmetrical ripple marks on bedding planes, indicating unidirectional current activity. The ripples exhibit distinct stoss and lee sides, with the stoss slope gently inclined (~15°, oriented towards N170) and the lee side relatively steeper (~30°, oriented towards N350), reflecting paleocurrent direction (Fig. 8a).

The rippled sandstone surface displays well-developed asymmetrical ripple marks preserved on

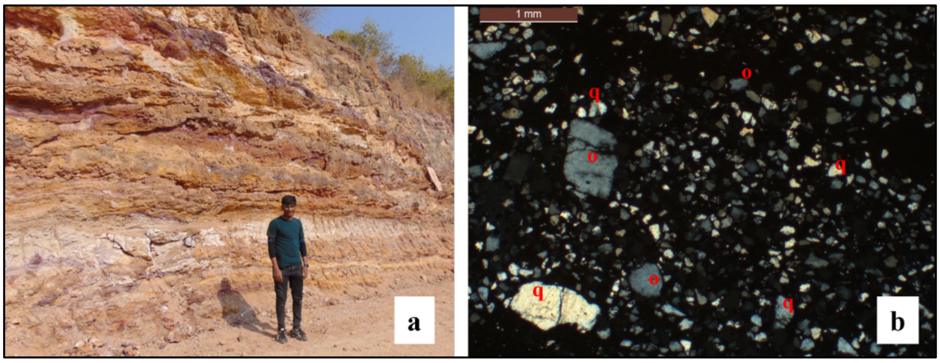

Fig. 9. Ferruginous sandstone facies: (a) Field photograph showing presence of thickly bedded fine grained sandstone unit of Katesar Member; (b) Photomicrograph of sandstone with medium to coarse angular grains of monocrystalline quartz (q), orthoclase (o), microcline (m), embedded in siliceous matrix and cemented by calcareous cementing material (XPL) (height of person: 170cm and hammer size: 30cm)

bedding planes. The ripples are laterally continuous and exhibit a clear distinction between gently inclined stoss slopes and relatively steeper lee slopes, indicating formation under unidirectional current flow. The crests are moderately sinuous to sub-linear and show consistent orientation across the exposed surface, suggesting stable flow conditions during deposition. Based on the hammer scale (30 cm), the ripple wavelengths are estimated to range between 28-30 cm, with amplitudes of approximately 5-7 cm, yielding ripple index (RI) values of ~5. The asymmetry of the ripples indicates sediment transport direction towards the lee side, reflecting tractional processes under lower flow regime conditions. The preservation of these bedforms suggests rapid burial and minimal post-depositional disturbance.

Conglomerate Facies (CO)

Field Characteristics:

The conglomerates occur as laterally discontinuous to locally persistent patches with a maximum exposed thickness of ~1 m. They are dark brown, compact and predominantly composed of granule- to pebble-sized quartz clasts with minor lithic fragments, indicating an oligomictic composition. The clasts are sub-rounded to rounded and exhibit moderate to poor sorting (Fig. 8b). The conglomerates display a matrix-supported to locally clast-supported fabric, with a coarse sandy matrix and ferruginous cement imparting the characteristic brown coloration. Trace fossils such as *Phycodes* (Desai, 2016) are observed within these units, indicating episodic colonization of the substrate under relatively stable conditions following high-energy depositional events.

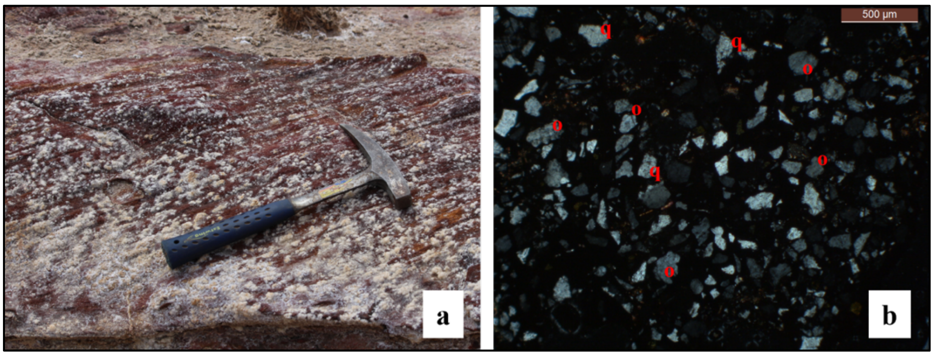

Fig. 10 Planar cross bedded sandstone facies: (a) Field photograph showing presence of planar cross stratifications in ferruginous sandstones; (b) Photomicrograph of sandstone with medium to coarse angular grains of monocrystalline quartz (q) and orthoclase (o) embedded in siliceous matrix and cemented by ferruginous cementing material (XPL) (hammer size: 30cm).

Ferruginous Sandstone Facies (FES)

Field Characteristics:

This facies is dominated by ferruginous sandstones that are medium- to fine-grained and exhibit pale red coloration on weathered surfaces and reddish-brown colour on fresh surfaces (Fig. 9a). The sandstones locally display lighter coloured bands; however, these are interpreted as the result of differential weathering rather than primary compositional variation. The lighter bands are likely formed due to localized alteration of iron-bearing minerals and development of limonitic patches under weathering conditions, giving a false impression of calcareous interbeds.

Petrography:

Petrographic analysis reveals sub-angular to sub-rounded, fine- to medium-grained (0.125–0.5 mm) framework grains with moderate sorting. The detrital composition is dominated by monocrystalline quartz (~92%), with subordinate feldspars (~5%) and minor lithic fragments (~3%) (Fig. 9b**)**. The grains exhibit tangential grain-to-grain contacts and show moderate sorting. The grains are embedded in a siliceous matrix and are cemented by ferruginous cementing material. The modal composition is Q92F5L3 (quartz 92%, feldspar 5%, lithic fragments 3%). Based on the proportion of framework grains and matrix, these sandstones are classified as 'Quartz arenites' (Dott, 1964).

Planar Cross-bedded Sandstone Facies (PCBS)

Field observations:

This facies comprises light brown to reddish, medium-grained sandstones. The dominant sedimentary structure is planar cross-bedding, developed as tabular sets with variable foreset dip angles reflecting migration of bedforms under unidirectional flow conditions (Fig. 10a). The cross-beds show consistent orientation, indicating stable paleocurrent conditions during deposition.

Petrography:

Petrographic analysis reveals sub-angular to sub-rounded, medium- to coarse-grained (0.25–1 mm) framework grains with moderate to well sorting, indicating textural submaturity. Grain contacts are predominantly tangential. The detrital composition is dominated by quartz (~88%), with subordinate feldspar (~8%) and minor lithic fragments (~4%) (Q88F8L4) (Fig. 10b). The framework grains are supported by a matrix and cemented by ferruginous material. The framework grains are embedded in a siliceous matrix and are cemented by ferruginous cementing materials. Based on the proportion of framework grains and matrix, these sandstones are classified as 'Subarkosic arenites' (Dott,1964).

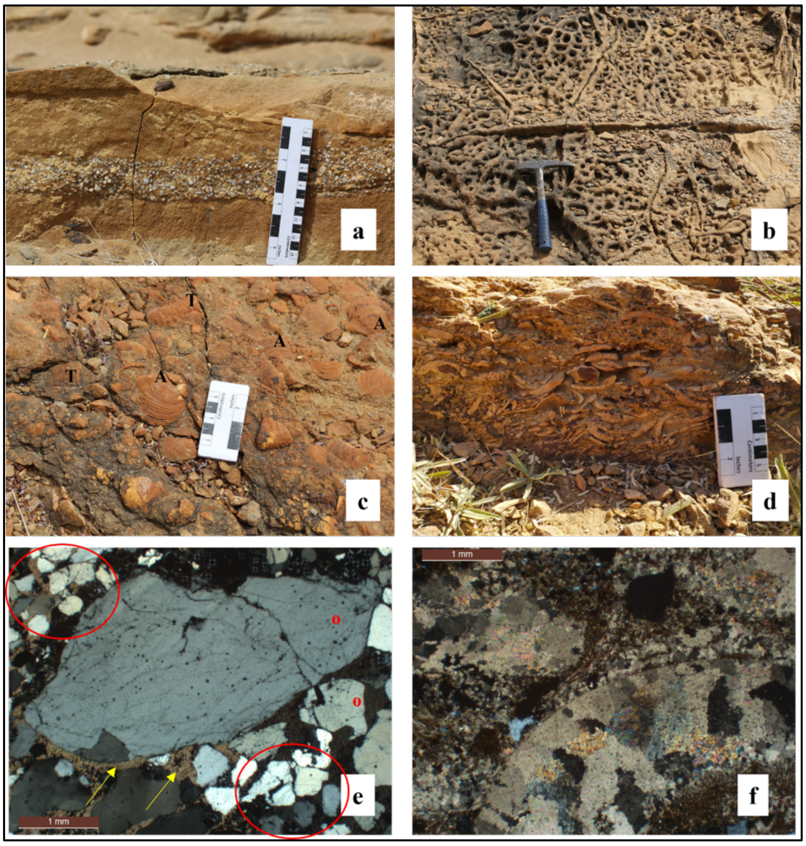

Fig. 11 (a) Field photograph showing pebbly sandstones; (b) Top surface shows presence of Thalassinoides; **(c)**, (d) Field photograph showing fossiliferous sandstones represented by of shells of Trigonia and Astarte on the top of the bed; (e) Photomicrograph of pebbly sandstone with coarse subangular grains of orthoclase (o), embedded in sandy matrix (red circles) and cemented by calcareous cementing material (yellow arrows); (f) Photomicrograph of fossiliferous sandstones showing replacement of micrite by sparite in the shell fragments. (XPL) (scale size short: 5cm and long: 30cm; hammer size:30cm)

Pebbly Sandstone Facies (PS)

Field Characteristics:

This facies comprises yellow to buff-coloured sandstones containing distinct bands of granule- to pebble-sized clasts (Fig. 11a). These coarse-grained horizons recur vertically within the unit and are interbedded with comparatively finer sandstone layers, producing a weakly stratified to graded profile. The clasts are rounded to sub-rounded, moderately sorted, and occur within a sandy matrix, with fabric varying from clast-supported to matrix-supported.

A bedding-plane view (Fig. 11b) shows a well-developed network of branching and interconnected tubular burrows attributable to *Thalassinoides*. These structures occur as irregular, horizontally to obliquely oriented galleries, indicating colonization of a relatively stable substrate following deposition.

Petrography:

Thin section analysis reveals moderate sorting with sub-rounded to rounded framework grains. The detrital composition is dominated by monocrystalline and polycrystalline quartz (~85–90%), with subordinate lithic fragments (~5–10%). The lithic fragments include fine-grained sedimentary and minor metamorphic rock fragments. The framework grains are supported by a fine-grained matrix, and cementation is variable (Fig. 11 e).

Fossiliferous Sandstones Facies (FS)

Field Characteristics:

This facies forms the uppermost unit of the Jhuran Formation and is laterally continuous over several tens of meters, with a maximum thickness of ~1 m. It comprises compact, coarse-grained calcareous sandstones containing abundant bivalve shells, predominantly *Trigonia* and *Astarte* (Fig. 11c, d).

The shells are mostly disarticulated and occur in random to weakly aligned orientations, suggesting episodic reworking under moderate energy conditions. Shell concentrations are higher in the upper parts of beds. The red colouration on account of ferrugination is locally observed on shell surfaces, indicating post-depositional oxidation.

Petrography:

Under the microscope, these sandstones show a mixed siliciclastic-carbonate nature wherein the siliciclastic detrital grains (55–60%) are moderately sorted and include coarse-grained (>1 mm) subrounded to subangular monocrystalline quartz and orthoclase feldspars (Fig. 11f). The carbonate components (30–45%) consist of allochems such as fragmented shells of bivalves. The carbonate cement is primarily represented by microcrystalline calcites with evidence of diagenetic alteration in the form of recrystallised grains of sparite within shell fragments. Based on composition and texture, the sandstones are classified as Allochemic Sandstones (Mount, 1985).

DIAGENESIS

Diagenetic features observed in the Katesar Member indicate early-stage modification under shallow burial conditions, supported by petrographic and field-based evidence.

A. Early Cementation: Early cementation is evidenced by the presence of ferruginous and calcareous cements observed in thin sections (Fig. 3b, 4b, 5b, 6c, 6d, 7b, 9b, 10b, 11e, 11f). The ferruginous cement occurs as pore-filling and grain-coating phases, imparting reddish-brown coloration due to precipitation of iron oxides under oxidizing pore-water conditions, whereas calcareous cement is present as sparry calcite filling intergranular pore spaces and replacing skeletal components in fossiliferous facies. The occurrence of these cements within relatively uncompacted grain frameworks indicates precipitation during early diagenesis (Burley et al., 1985; Morad et al., 2000; Worden and Morad, 2003).

B. Minimal Mechanical Compaction: Mechanical compaction is limited, as indicated by the predominance of tangential and floating grain contacts (Fig. 7b, 9b, 10b), with only occasional concavo–convex contacts. The absence of pressure solution features such as sutured contacts or stylolites suggests shallow burial conditions and early stabilization of the sediment framework (Burley et al., 1985; Boggs, 2009). Early cementation played a key role in inhibiting significant compaction and preserving primary textural maturity.

C. Preservation of Detrital Mineralogy: Preservation of detrital mineralogy is reflected by the abundance of fresh monocrystalline quartz, feldspar grains, and identifiable lithic fragments, with minimal evidence of chemical alteration or replacement. Such preservation indicates that diagenetic overprinting has not significantly modified the primary mineral assemblage, consistent with early diagenetic (eogenetic) conditions (Morad et al., 2000; Worden and Burley, 2003).

D. Preservation of Primary Structures: Features such as ripple marks (Fig. 8a), laminations (Fig. 7a), fining-upward trends and clast-supported fabrics (Fig. 8b) are well preserved, indicating that lithification occurred early enough to resist later compaction. Bioturbated facies however, show post-depositional alteration of primary fabrics due to biological reworking, yet stabilization through cementation still occurred at shallow burial depths.

E. Influence of Pore-Water Chemistry: Diagenesis reflects strong control of fluctuating pore-water chemistry with localized variability between iron-rich oxidizing conditions and carbonate-saturated marine fluids. The alternation of ferruginous and calcareous cementation types indicates dynamic geochemical conditions that varied spatially and temporally across the depositional system (Burley et al., 1985; Worden and Morad, 2003).

F. Role of Biogenic Activity: In several facies, the presence of trace fossils (e.g., Skolithos, Thalassinoides, Phycodes) (Fig. 5a, 11b) and bioclastic debris (e.g., Trigonia, Astarte shells) (Fig. 11 c, d) reveals biological influence on diagenesis. The bioturbation enhanced pore-fluid circulation pathways, while the bioclastic fragments contributed significantly to the carbonate content, which later recrystallized from micrite to sparite during progressive chemical diagenesis (Burley et al., 1985; Flügel and Munnecke, 2010).

Overall, the diagenetic features which include early cementation, limited compaction, preservation of

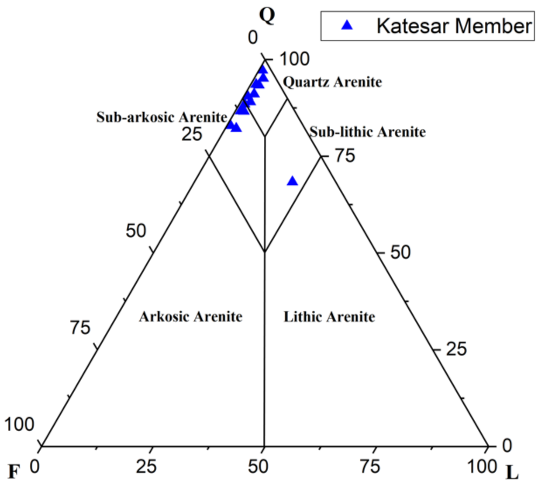

Fig. 12 QFL plot showing classification of sandstones (after Dott, 1964)

detrital mineralogy, and absence of deep burial indicators are consistent with eogenetic diagenesis operating under shallow burial conditions (Morad et al., 2000; Worden and Morad, 2003).

HEAVY MINERAL STUDIES

The sandstone samples representing all facies from the Katesar Member display a moderately to well-developed assemblage of heavy minerals (Table 3), comprising both opaque and non-opaque varieties. Opaque minerals form a significant portion of the assemblage. The non-opaque heavy minerals identified include rutile, zircon, garnet and tourmaline (Fig. 13). The grain size varies from fine to medium and the grains are subangular in nature. The heavy minerals suite comprises opaque > zircon > rutile > tourmaline> garnet in order of abundance.

The properties of the examined heavy minerals are described in Table 3 as follows:

Table 3: Heavy Mineral Properties

Zircon:	Colorless to pale brown in thin section, high relief, and high order interference color.
Rutile:	Euhedral, red to deep-blooded colored, pleochroism in shades of red, high relief.
Tourmaline:	Pleochroism- dark green to pale yellow, moderate relief, high order interference color.
Garnet:	Euhedral grains, high relief, isotropic, and grey or white interference color.

BULK MINERALOGY

Representative sandstone samples from the Katesar Member were analyzed for bulk mineralogy using X-ray diffraction (XRD). The analysis revealed that the sandstones contain clay and non-clay minerals, as identified through the XRD results. The rocks from the Katesar Member exhibit a range of clay and non-clay minerals. The clay minerals observed include kaolinite, montmorillonite and vermiculite, while the non-clay minerals consist of quartz, calcite, orthoclase, muscovite, microcline, goethite, and hematite (Table 4, Fig 14). Quartz remains a significant component, followed by feldspars and iron oxides.

Table 4: Clay and non-clay minerals from Katesar Member of Jhuran Formation

Formation	Member	Facies	Non-clay minerals	Clay minerals
Jhuran	Katesar	Fossiliferous Sandstone Facies	Quartz, Microcline, Muscovite	Kaolinite
		Pebbly sandstone Facies	Quartz, Hematite, Muscovite, Orthoclase	Glauconite, Kaolinite
		Planar Cross bedded Sandstone Facies	Quartz, Orthoclase, Muscovite, Goethite, Calcite	Kaolinite
		Rippled sandstone Facies	Quartz, Muscovite, Orthoclase, Goethite	Kaolinite
		Conglomerate Facies	Quartz, Muscovite, Orthoclase	Kaolinite, Vermiculite, Montmorillonite
		Thinly bedded sandstone Facies	Quartz, Orthoclase, Muscovite, Goethite, Calcite	Kaolinite
		Intercalated shale-siltstone Facies	Quartz, Hematite, Muscovite, Orthoclase	Kaolinite
		Bioturbated sandstone Facies	Quartz, Hematite, Goethite, Muscovite,	Kaolinite
		Hummocky cross stratified sandstones Facies	Quartz, Orthoclase, Microcline, Calcite	Kaolinite
		Gypsiferous shale Facies	Quartz, Microcline, Calcite, Gypsum,	Kaolinite, Glauconite, Vermiculite, Montmorillonite

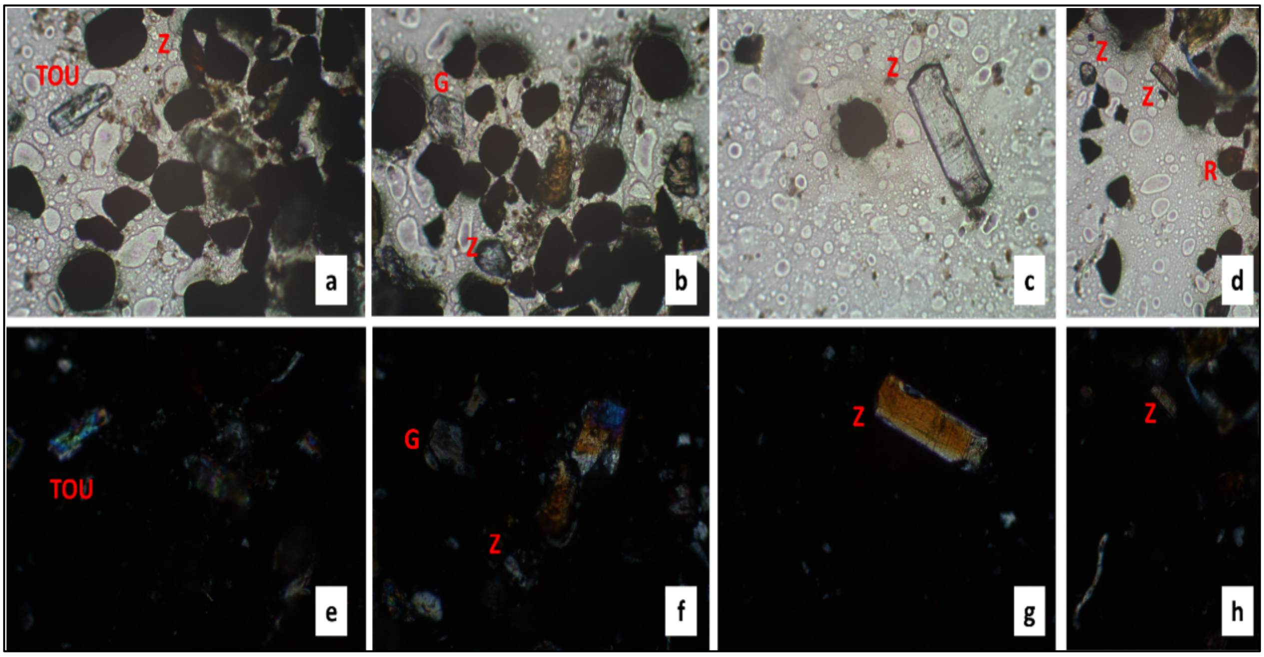

Fig. 13 Photomicrographs of heavy minerals from Katesar Member (a), (e) Tourmaline and Zircon under ppl and Xpl. (b), (f) Garnet and Zircon under ppl and Xpl. (c), (e) Zircon under ppl and Xpl. (d), (h) Zircon and Rutile ppl and Xpl. [ppl = plane polarized light, Xpl = cross-polarized light, R = rutile, Z = zircon, Tou = tourmaline, G = garnet]

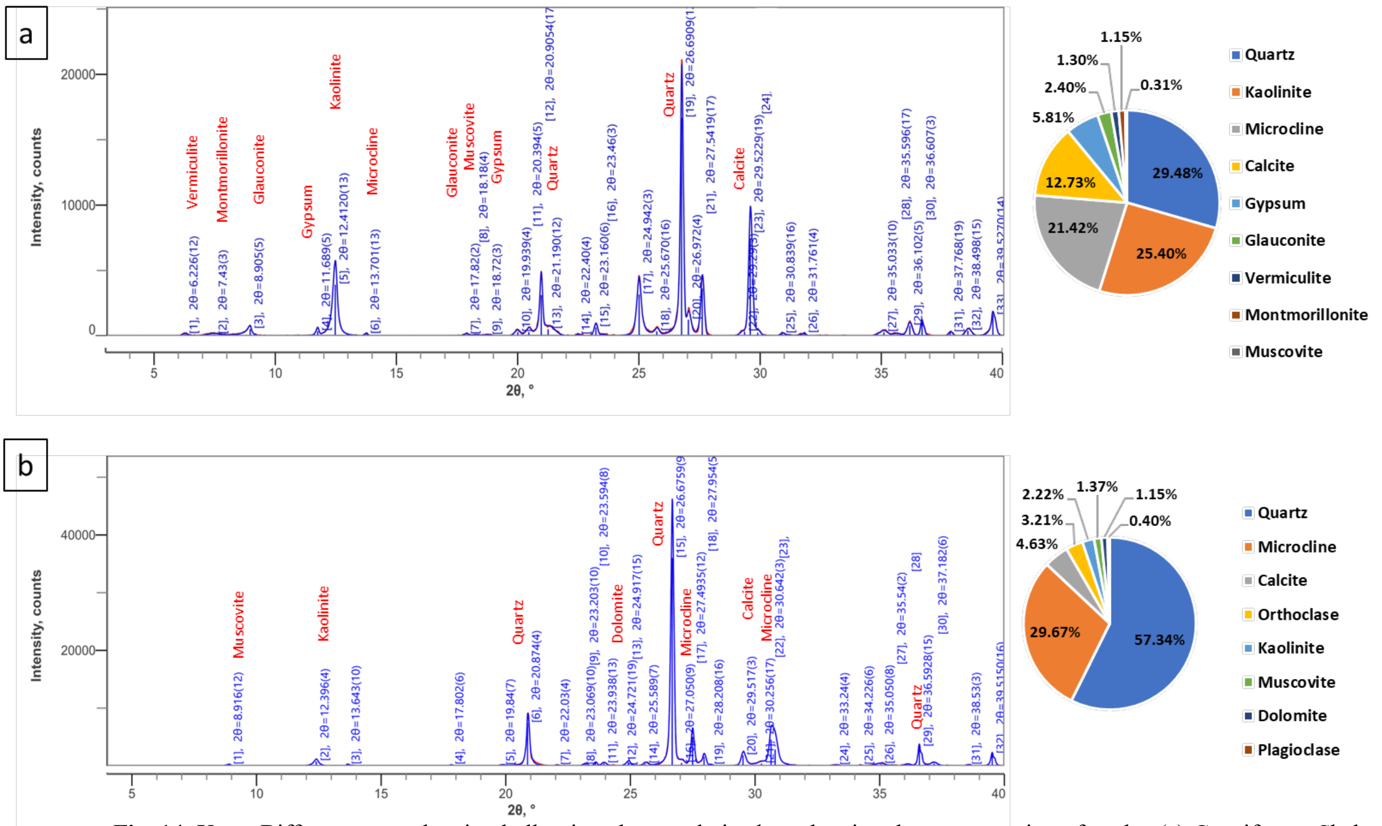

Fig. 14. X-ray Diffractograms showing bulk mineralogy and pie chart showing the concentration of peaks: (a) Gypsiferous Shale facies (b) Pebbly Sandstone facies

GEOCHEMISTRY

The representative samples of the Katesar Member have been analyzed for major oxides using Wavelength Dispersive X-Ray Fluorescence (WD-XRF). The major element oxide results of the studied sandstones are presented in Table 5. The SiO_2 content of sandstone ranges between 40.28% and 73.15%, along with TiO_2 (0.10 to 0.86), Al_2O_3 (0.98 to 10.76), Fe_2O_3 (0.90 to 32.53), MnO (0.06 to 0.10), MgO (0.13 to 2.95), CaO (0.05 to 2.01),

Na_2O (0.68 to 9.81), K_2O (0.01 to 0.62), and P_2O_5 (0.05 to 1.40). The order of abundance of major oxides is SiO_2 followed by Al_2O_3, CaO, MgO, Fe_2O_3, Na_2O, K_2O, TiO_2, P_2O_5, and MnO. The presence of CaO and Fe_2O_3 is significant in comparison with other oxides and suggests higher proportions of carbonates and iron-bearing components.

TRACE ELEMENTS

The representative samples from the lithofacies of the Katesar Member have been subjected to trace elemental analysis (Table 6). The concentration of trace elements within rocks of the Katesar Member shows similar concentrations in comparison to Upper Continental Crust (UCC) and Post Archean Australian Shale (PAAS) values (Fig. 15). The concentrations of High Field Strength Elements (HFSEs) such as Zr, Hf, Y, and Nb along with Large Ion Lithophile Elements (LILEs) such as Rb, Sr, Cs, Ba, Th, and U are broadly comparable and follow the UCC and PAAS trends; however, Rb, Zr and Ba shows depletion. The similarity in the concentrations of HFSE within the rocks of the Katesar Member is suggestive of similar zircon input or recycling intensity. The depletion in the values of Zr indicates limited zircon contribution or lower maturity and that of Rb and Ba suggests a weathered or recycled sediment source. The concentration of Trace Transition Elements (TTEs) such as Cr, Ni, Sc, Cu, and V is low and exhibits a slightly depleted pattern relative to UCC and PAAS values. The lower concentrations of TTE than UCC and PAAS, suggest a depleted or highly weathered source.

This comparison exhibits overall consistency with post-Archean upper continental crust signatures, with minor variations reflecting subtle differences in provenance and sediment composition.

DISCUSSION

The results obtained from petrography, geochemistry, and heavy mineral studies have been interpreted to classify the rocks of the Katesar Member and evaluate the provenance, tectonic settings, paleoclimate, and paleoenvironment, as discussed below.

Table 5: Major and Minor oxides concentration (in %) in lithofacies of Katesar Member (GS-FES) of Jhuran Formation.

Facies / Oxides	GS	HCSS	BFS	ISHS	TBSS	RS	CO	FES
SiO_2	73.15	40.06	40.28	48.99	62.67	65.17	68.28	66.41
TiO_2	0.10	0.20	0.36	0.33	0.55	0.86	0.19	0.41
Al_2O_3	0.98	10.76	4.70	4.20	6.06	9.48	1.55	8.21
Fe_2O_3	5.24	18.78	32.53	8.69	3.15	4.87	6.92	0.90
MnO	0.10	0.08	0.07	0.13	0.06	0.10	0.08	0.09
MgO	0.20	0.13	0.26	2.95	0.35	0.37	0.16	0.22
CaO	0.10	0.20	0.20	2.01	0.05	0.16	0.47	0.10
Na_2O	0.68	9.81	0.59	0.81	1.81	0.83	0.81	0.87
K_2O	0.01	0.01	0.29	0.62	0.28	0.55	0.29	0.20
P_2O_5	0.04	1.40	0.05	0.07	0.07	0.08	0.00	0.06
LOI	19.40	18.60	20.21	30.89	24.66	16.70	21.04	22.61
Total	99.99	99.7	99.53	99.68	99.71	99.17	99.78	100.0

Table 6: Trace element concentration in lithofacies of Katesar Member (GS-FES)

Element	Isotope	BHVO-2 USGS		HCSS	BFS	ISHS	TBSS	RS	CO	FES
		Rep.	Meas.							
Sc	45Sc	31.8	31	2.98	2.92	16.3	1.43	3.74	13.1	1.41
V	51V	318	304	31.4	18.4	253	51.6	69.6	95.5	24.6
Cr	52Cr	287	285	21.1	14.2	124	25.4	22.5	281	16.8
Co	59Co	44.9	44.8	10.8	46.9	14.3	24.9	49.7	57.7	53.7
Ni	60Ni	120	120	39.7	11.9	25.2	9.2	14.2	65.5	13.2
Cu	63Cu	129	134	10.4	8.9	14.4	29.0	14.3	18.7	8.7
Zn	66Zn	104	110	62.4	34.7	324	58.4	61.5	120	67.6
Rb	85Rb	9.26	9.17	63.0	39.1	30.9	32.6	28.5	31.1	18.8
Sr	88Sr	394	396	106	151	1050	198	155	43.8	36.8
Y	89Y	25.9	25.6	4.71	7.93	28.7	5.42	8.43	17.4	5.35
Zr	90Zr	171	159	31.9	40.5	105	24.7	47.2	122	66.1
Nb	93Nb	18.1	14.3	4.93	1.71	12.5	1.47	1.34	10.7	3.06
Cs	133Cs	0.10	0.11	0.54	0.24	1.51	0.38	0.38	1.70	0.56
Ba	137Ba	131	141	852	606	126	319	260	188	290
La	139La	15.2	15.2	9.17	9.88	58.2	11.2	13.0	31.1	18.5
Ce	140Ce	37.5	38.1	19.7	19.7	157	22.5	28.9	61.3	35.7
Pr	141Pr	5.34	5.41	2.04	1.90	22.2	2.62	3.13	7.63	4.08
Nd	146Nd	24.3	24.0	8.09	6.24	81.5	9.54	11.0	27.2	13.9
Sm	147Sm	6.02	6.14	1.60	1.04	14.3	1.90	2.08	5.76	2.69
Eu	153Eu	2.04	2.15	0.79	0.61	2.59	0.48	0.52	1.12	0.42
Gd	157Gd	6.21	6.48	1.47	1.39	16.0	1.88	1.93	5.50	2.48
Tb	159Tb	0.94	0.97	0.18	0.20	2.01	0.21	0.26	0.73	0.26
Dy	163Dy	5.28	5.44	0.96	1.38	7.72	1.14	1.34	4.05	1.37
Ho	165Ho	0.99	1.03	0.18	0.30	1.16	0.23	0.28	0.75	0.24
Er	166Er	2.51	2.70	0.49	0.84	2.54	0.57	0.65	2.23	0.63
Tm	169Tm	0.33	0.37	0.08	0.13	0.26	0.07	0.11	0.32	0.10
Yb	172Yb	1.99	2.10	0.38	0.69	1.51	0.41	0.55	2.19	0.65
Lu	175Lu	0.28	0.29	0.06	0.10	0.17	0.07	0.08	0.36	0.11
Hf	178Hf	4.47	4.49	1.23	1.01	2.68	0.91	1.29	4.45	2.38
Ta	181Ta	1.15	1.17	0.22	0.11	0.76	0.08	0.06	0.65	0.08
Th	232Th	1.22	1.24	3.49	2.1	24.1	4.40	4.18	17.5	10.4
U	238U	0.42	0.45	0.92	0.62	3.38	0.58	0.71	5.61	1.48

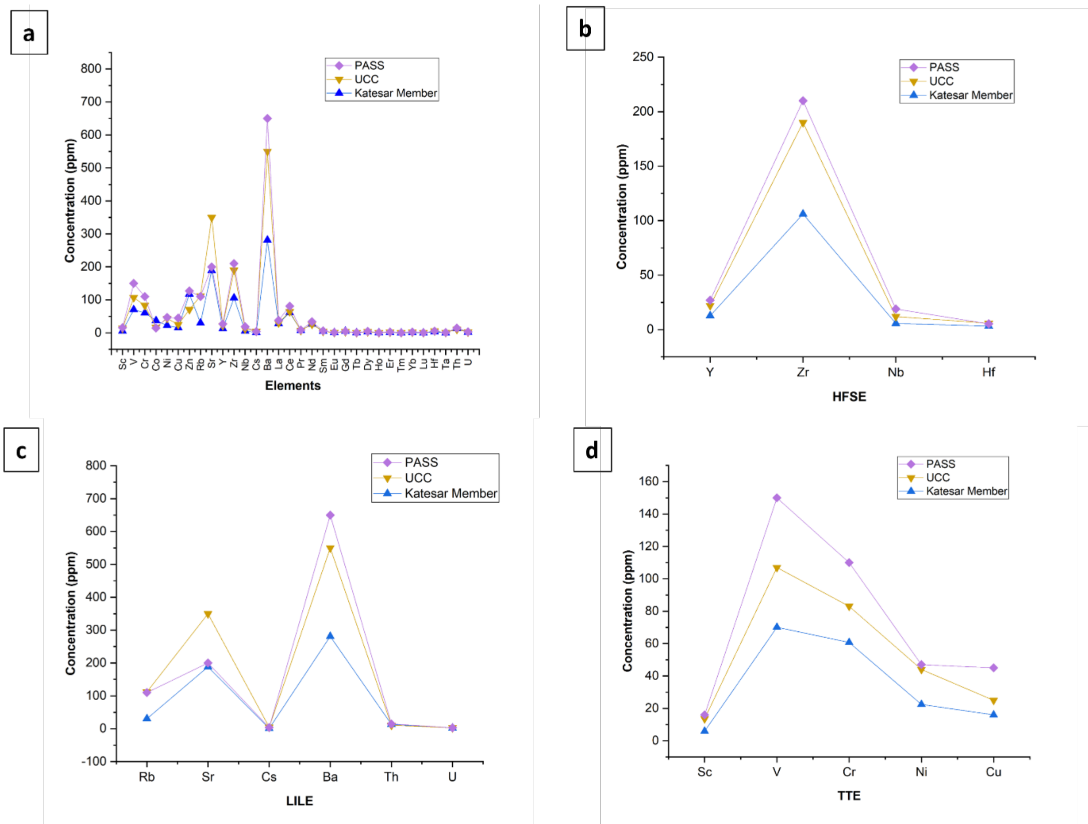

Fig. 15 Trace element concentration in the middle and upper Katesar Member of Jhuran Formation (a) Concentration of elements in comparison to UCC and PAAS. (b) Concentration of High Field Strength Elements (HFSE). (c) Concentration of Trace Transition Elements (TTE). (d) Concentration of large Ion Lithophile Elements (LILE).

GEOCHEMICAL CLASSIFICATION

The chemical classification proposed by Herron (1988) based on oxide data serves as a valuable proxy for classification of clastic rocks. This approach involves the use of ratios of log (Fe_2O_3/K_2O) vs log (SiO_2/Al_2O_3) and is particularly helpful in distinguishing between various clastic rock types such as sandstone and shale or quartz arenite and lithic arenite especially in cases where textures have been modified or obscured by diagenetic processes.

The sandstones of the Katesar Member, based on their matrix content and proportion of framework grains, have been classified as quartz arenites, sub-lithic arenites and sub-arkosic arenites (Dott, 1964). The overall Al_2O_3 content (3.24–28.87 wt%, average ~11.3 wt%), K_2O (0.37–1.79 wt%, average ~0.88 wt%), and Na_2O (0.58–7.82 wt%, average ~2.49 wt%) indicate the presence of both K-feldspars and plagioclase feldspars which is in concurrence with the petrographic observations. The average CaO content (9.71 wt%) suggests the development of diagenetic calcareous constituents while the Fe_2O_3 content (average 4.47 wt%) indicates precipitation of iron oxides like limonite or goethite under oxidizing conditions.

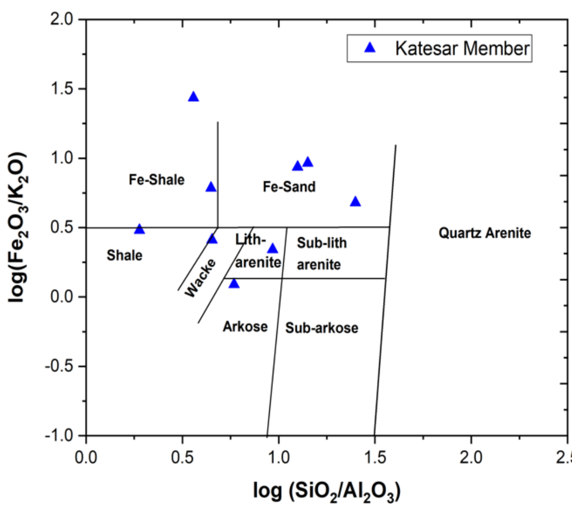

Fig. 16 Geochemical classification based on log (Fe_2O_3/K_2O) vs. log (SiO_2/Al_2O_3) plot after Herron (1988)

The chemical classification (Herron, 1988) (Fig. 16) indicates wacke, lithic arenite, and Fe-sand varieties for these sandstones. The variations in the sandstone types observed from this plot as compared to (Dott, 1964) (Fig. 12) are attributed to the high Fe_2O_3 concentration on account of the presence of ferruginous cement formed by diagenetic changes under oxidizing and reducing conditions during deposition.

PALAEO-WEATHERING CONDITIONS

The intensity of chemical weathering in source rocks depends on their composition, duration of exposure, climatic conditions, and tectonic uplift (Nesbitt and Young, 1982; McLennan, 1993; Ghaznavi et al., 2018). During weathering, labile minerals such as feldspars and volcanic glass are transformed into clay minerals, leading to the depletion of Ca, Na, and K (Taylor and McLennan, 1985; Fedo et al., 1995). The residual concentrations of these elements, along with alkali ratios ($K_2O + Na_2O$; K_2O/Na_2O), reflect the degree of weathering (Lindsey, 1999).

Weathering intensity is commonly quantified using indices such as the Chemical Index of Alteration (CIA), Chemical Index of Weathering (CIW), and Plagioclase Index of Alteration (PIA). CIA values range from ~50 for unweathered to ~100 for completely weathered rocks, indicating progressive leaching of Ca, Na, and K (Nesbitt and Young, 1982; Sun et al., 2013). The CIW provides a similar measure using fewer components (Harnois, 1988), while the PIA tracks feldspar alteration to clay minerals (Fedo et al., 1995). The Index of Compositional Variability (ICV; Cox et al., 1995) and SiO_2/Al_2O_3 ratio further assess sediment maturity—ICV > 1 suggests mineralogical immaturity and tectonic activity, whereas ICV < 1 reflects compositional maturity (Verma and Armstrong-Altrin, 2013).

For the Katesar Member, CIA values range from 39.58–92.03 (avg. 67.88), CIW from 41.30–97.51 (avg. 72.35), and PIA from 9.63–46.05 (avg. 22.51), indicating moderate to intense chemical weathering and partial feldspar alteration. ICV values (0.42–9.51; avg. 2.15) imply first-cycle deposition with enrichment in rock-forming minerals, while SiO_2/Al_2O_3 ratios (1.79–25.01; avg. 9.26) indicate variable compositional maturity.

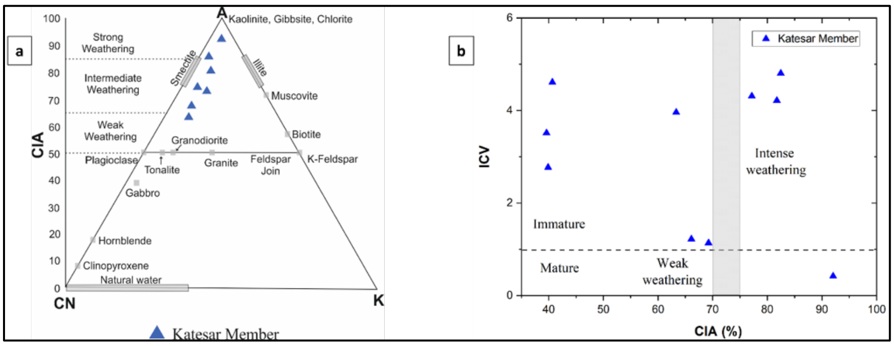

Fig. 17 (a) A–CN–K ternary diagram showing degree of alteration (after Nesbitt and Young, 1982); (b) ICV versus CIA bivariate diagram representing maturity and weathering nature (after McLennan et al., 1993).

The ICV-CIA relationship suggests moderate to moderately high weathering intensity and overall moderate maturity (Fig. 17).

PALEOCLIMATE

Sandstone petrography and major oxide geochemistry are used to infer paleoclimatic conditions, as sandstone composition is influenced by climate-controlled weathering processes (Suttner et al., 1981; Suttner and Dutta, 1986). Humid climatic conditions enhance chemical weathering, leading to enrichment of quartz relative to feldspar and lithic fragments. To evaluate paleoclimate, QFL modal data were plotted on the ternary diagram of Suttner et al. (1981), and detrital components were further analyzed using Qp/(F+L) and Qt/(F+L) ratios on log–log

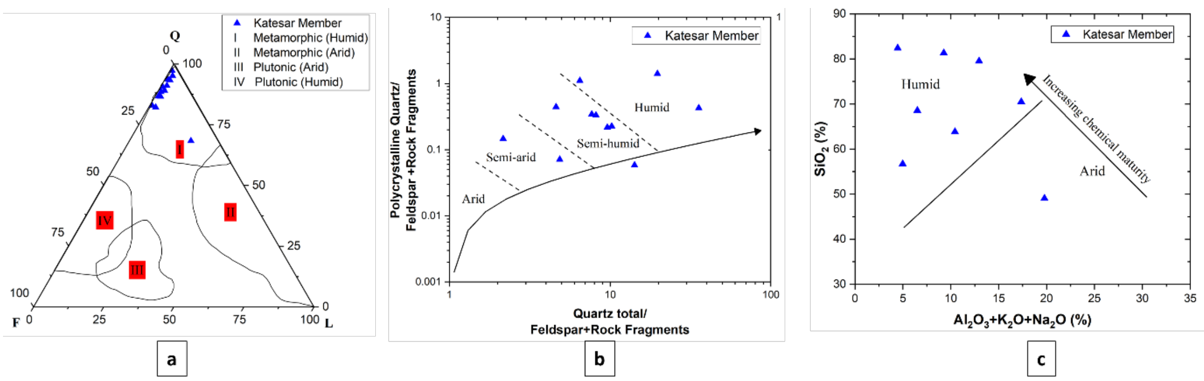

Fig. 18 (a) Q-F-R ternary diagram showing paleoclimate (after Suttner et al., 1981) (b) Binary plot of log Qp/(F+L) and Qt/(F+L) (after Suttner and Dutta, 1986) c Binary plot of SiO_2 versus Al2O3+K2O+Na2O showing chemical maturity (after Suttner and Dutta, 1986)

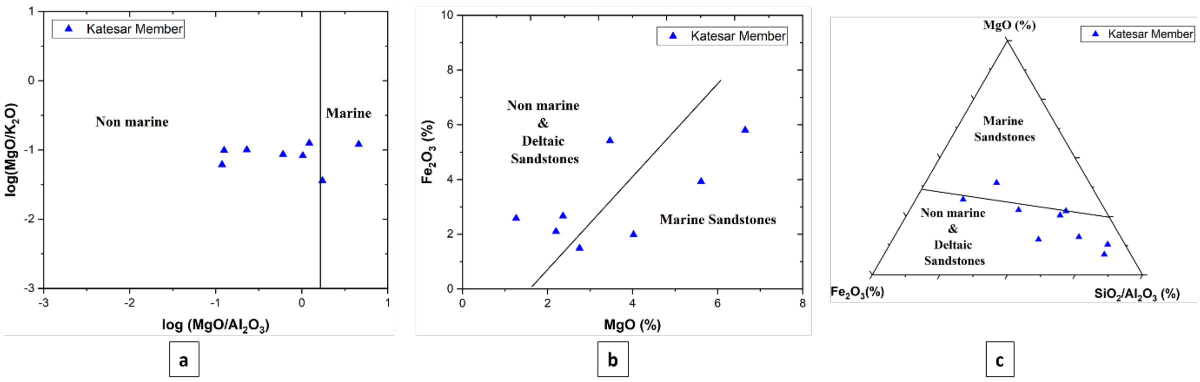

Fig. 19 (a) Binary plot of log (MgO/Al_2O_3) versus log (K_2O/Al_2O_3) to interpret the depositional environment (after Roaldest, 1978) (b) Binary plot of Fe_2O_3 versus MgO representing conditions prevailing during deposition (after Ratcliffe, 2007) (c) MgO- Fe_2O_3- SiO_2/Al_2O_3 Ternary plot representing environmental conditions (after Ratcliffe, 2007).

plots (Suttner and Dutta, 1986). In addition, major oxide data were examined using the SiO_2 vs. (Al_2O_3 + K_2O + Na_2O) relationship to constrain climatic conditions. The results of these analyses are presented below.

The modal analysis for sandstones of Katesar Member indicate their derivation from metamorphic sources rocks and their deposition in humid paleoclimatic conditions (Fig. 18). This is in concurrence with the semi-arid to humid climatic zone in the bivariate plot of SiO_2 vs. Al_2O_3 + K_2O + Na_2O (Suttner and Dutta, 1986) (Fig.18). The bulk mineralogical analysis indicates the predominant presence of kaolinite in the sediments, which reflects the low salinity of the depositing medium (Manker and Griffin, 1971). It usually forms from the weathering of granites under warm and humid climatic conditions (Mozherovsky and Terekhov, 1998). The values indicate moderate chemical maturity, reflecting a sub-humid to semi-arid climate with periodic enhancement in weathering.

PALEO-DEPOSITIONAL ENVIRONMENT

The paleoenvironmental conditions of the Katesar Member of the Jhuran Formation are interpreted using bulk mineralogical and geochemical data. Variations in major oxide composition, particularly Fe_2O_3 and MgO, are commonly used to distinguish between marine and non-marine depositional settings (Ratcliffe et al., 2007). Elevated values of these oxides may reflect the presence of Fe–Mg-bearing minerals such as carbonates and clay minerals, which are indicative of marine influence. The log values of (MgO/K_2O)/(MgO/Al_2O_3) have also been widely applied as an environmental discriminator, with values between 0.01 and 0.10 suggesting transitional conditions (Roaldest, 1978; Bhattacharjee et al., 2018).

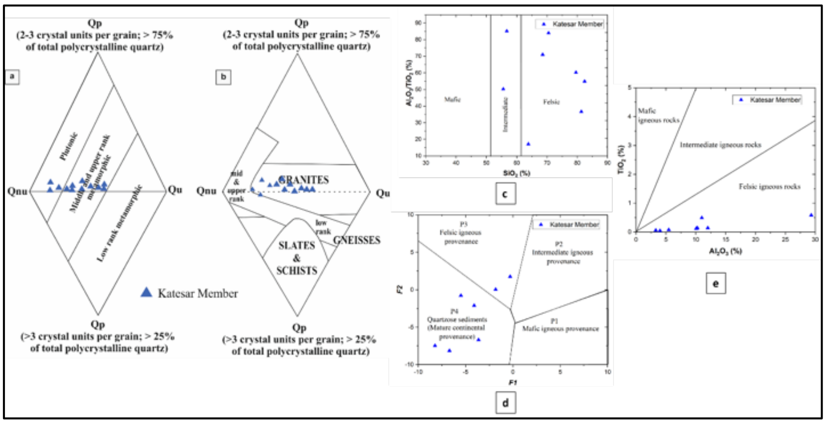

Fig. 20. Diamond diagrams (a) After Basu et al. (1975) (b) After Tortosa et al. (1991) of quartz types (c) Binary plot of SiO_2 versus Al_2O_3/TiO_2 (after Bas et al, 1986) (d) Binary plot of F1 versus F2 showing provenance (after Roser and Korsch, 1988) (e) Binary plot of TiO_2 versus Al_2O_3 (after Hayashi et al., 1997)

In the present study, log values of (MgO/K_2O)/(MgO/Al_2O_3) range from 0.09 to 1.7 (average ~0.55), suggesting predominantly non-marine to marginal marine (deltaic) conditions (Fig. 19). However, binary and ternary geochemical plots (Ratcliffe et al., 2007) indicate fluctuating conditions between marine and non-marine environments, reflecting a transitional depositional setting (Fig. 19).

The presence of glauconite within the rocks of the Katesar Member, observed in XRD studies, indicates a shallow marine environment possibly on account of alteration of biotite (Porrenga, 1967). The presence of goethite points to oxidizing conditions within the depositional medium, likely formed through the oxidation of sulfides during weathering (Zwing et al., 2005).

PROVENANCE

Provenance refers to the origin and source characteristics of sediments and can be inferred using petrographic, geochemical, and mineralogical approaches (Sengupta, 2017). The mineralogical composition of terrigenous sediments reflects the nature of the source rock and, to some extent, climatic and tectonic influences. In this study, provenance of the sandstones of the Katesar Member is evaluated using petrographic characteristics, including quartz typology (Basu et al., 1975; Dickinson et al., 1983; Dickinson, 1985), major oxide geochemistry (Roser and Korsch, 1988; Cullers, 2000), and trace element ratios (Bhatia, 1983; Cullers, 2000). Quartz types were plotted on diamond diagrams (Basu et al., 1975; Tortosa et al., 1991), while major and trace element data were analyzed using established discrimination diagrams and elemental ratios to constrain source rock composition and tectonic setting.

The results obtained from the quartz typology plots (Basu et al, 1975; Tortosa et al., 1991) for the sandstones of the Katesar Member indicate plutonic igneous provenance supplemented by middle to upper-grade metamorphic sources (Fig. 20). The high abundance of polycrystalline quartz and the presence of feldspars and muscovite grains further confirm their derivation from acidic igneous rocks such as granites.

The values of Al_2O_3/TiO_2 (Hayashi et al, 1997) ratio for these sandstones indicate a predominantly felsic igneous field (Fig. 20) whereas **on** the discriminant function plot (Roser and Korsch,1988), they cluster within the quartzose sediment field (P4), suggesting mature continental provenance. The presence of heavy minerals such as rutile and garnet reaffirms the metamorphic contribution. The binary plots of Th/Co vs La/Sc (Cullers, 2000), La/Th vs Hf (Floyd and Leveridge, 1987), Cr/V vs Y/Ni (McLennan et al.,1993) and Th/Sc vs Zr/Sc (McLennan et al.,1993) points to felsic source rocks, mainly granites (Fig. 21) which is also corroborated by binary plot (McLennan and Taylor, 1991) (Fig. 21).

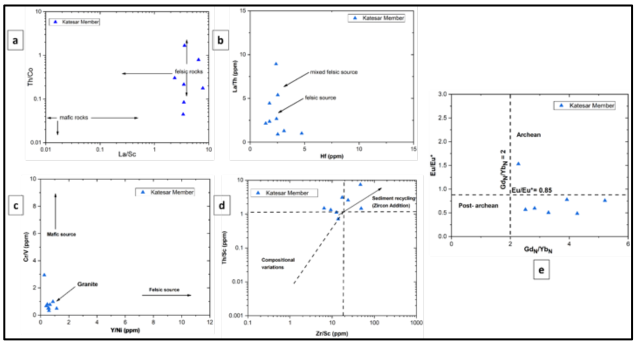

Fig. 21. a Binary plot representing provenance (a) Th/Co versus La/Sc (after Cullers, 2000) (b) La/Th versus Hf (after Floyd and Leveridge, 1987) (c) Cr/V versus Y/Ni (after McLennan et al., 1993) (d) Th/Sc versus Zr/Sc (after McLennan et al., 1993) (e) Eu/Eu* versus (Gd/Yb) CN (after McLennan and Taylor,1991)

TECTONIC SETTINGS

Tectonic setting of the source region can be effectively constrained using framework mineralogy and elemental geochemistry of clastic sediments (Dickinson and Suczek, 1979; Bhatia, 1983). In this study, modal data are plotted on QtFL and QmFLt diagrams (Dickinson et al., 1983), and major oxide compositions are evaluated using tectonic discrimination functions (Bhatia, 1983) to infer the tectonic setting during deposition.

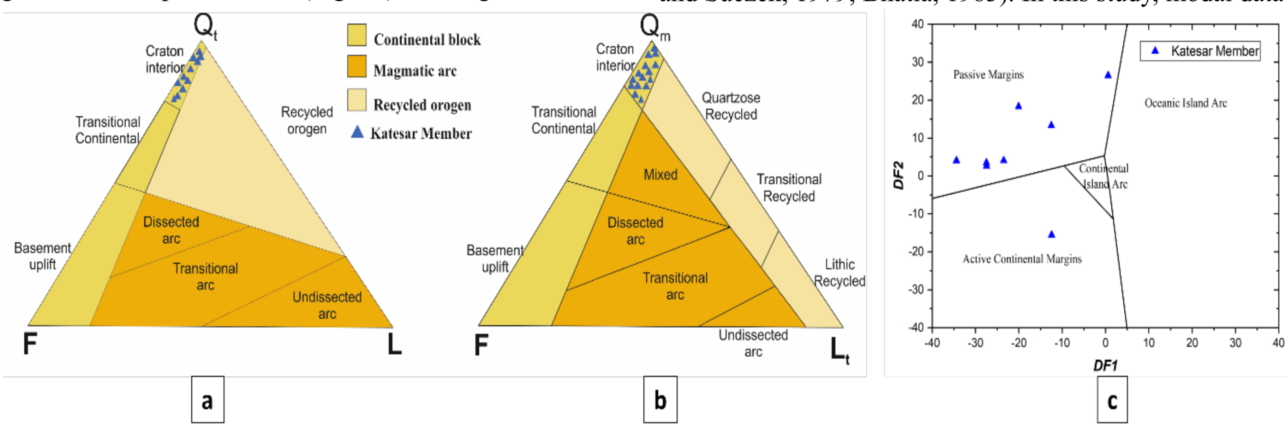

Fig. 22. (a) Q_tFL and (b) Q_mFL_t ternary diagrams after Dickinson et al. (1983). c Discriminant Function 2 versus Discriminant Function 1 binary plot (after Bhatia,1983).

The tectonic settings of Katesar Member based on QtFL and QmFLt plots (Dickinson et al., 1983) appear to be craton interior fields within a continental block (Fig. 22). This suggests their derivation from a stable basement terrain likely granitic in nature. The discriminant function (DF1–DF2) plot (Bhatia, 1983) (Fig. 22) further supports their deposition along passive margins which is indicative of a tectonically stable, intracratonic depositional basin.

CONCLUSIONS

The Katesar Member of the Jhuran Formation records the evolution of a progradational deltaic system developed along the margin of the Kachchh Basin during the Late Jurassic. Facies analysis reveals two principal depositional domains, namely a storm-influenced delta front and a fluvially dominated delta plain. The delta-front deposits, characterized by hummocky cross-stratification, bioturbation, and heterolithic facies, indicate sedimentation under fluctuating energy conditions with episodic marine influence. In contrast, the delta-plain deposits, comprising thinly bedded and rippled sandstones, gypsiferous shales, and conglomerates, reflect deposition in distributary channels, crevasse splays, levees, and interdistributary bays, with evidence of periodic subaerial exposure and variable hydrodynamic conditions.

Trace fossil assemblages, including *Skolithos*, *Thalassinoides*, and *Phycodes*, provide additional constraints on depositional energy and sedimentation rates, indicating alternating phases of rapid deposition and ecological colonization. Petrographic and mineralogical characteristics, supported by XRD and heavy mineral analyses, demonstrate quartz-dominated, compositionally mature sediments derived predominantly from felsic sources with evidence of recycling. Geochemical signatures, including major and minor oxide compositions, further corroborate a quartz-rich sediment supply under moderate weathering conditions.

The integration of sedimentological, ichnological, mineralogical, and geochemical data indicates progressive shoreline progradation and transition from marine-influenced delta-front conditions to predominantly fluvial delta-plain environments. This depositional evolution reflects increasing sediment supply and reduced accommodation, with intermittent marine incursions recorded by storm-generated structures and bioturbation. The study provides a comprehensive reconstruction of deltaic processes and contributes to understanding sediment dispersal and basin evolution in a rift-margin setting.

ACKNOWLEDGEMENTS

The authors are thankful to the Department of Geology, The Maharaja Sayajirao University of Baroda for the infrastructural facilities to carry out the present work. We express our gratitude to Sophisticated Instrumentation Centre for Applied Research and Testing (SICART), Anand, Gujarat for XRF facility, CEWELL, ONGC Vadodara for XRD analysis and Physical Research Laboratory (PRL) for ICP-MS analysis.

AUTHOR CONTRIBUTIONS

PM (Poonam Mangtani): Conceptualization, Investigation, Data analysis, Interpretation and Writing original draft. AVJ (A.V. Joshi): Supervision, Investigation and writing review and editing.

FUNDING

This research did not receive any specific grant from funding agencies in the public, commercial, or not-for-profit sectors.

DATA AVAILABILITY:

The author confirms that the data supporting the findings of this study are available within the article.

COMPETING INTEREST:

The authors have no competing interests to declare that are relevant to the content of this article.

REFERENCES

Arora, A., Banerjee, S., Dutta, S. (2015). Black shale in late Jurassic Jhuran Formation of Kutch: Possible indicator of oceanic anoxic event?; Journal of the Geological Society of India, v. 85(3), p.265-278.

Bas, M.L., Maitre, R.L., Streckeisen, A., Zanettin, B. (1986). IUGS Subcommission on the Systematics of Igneous Rocks. A chemical classification of volcanic rocks based on the total alkali-silica diagram; Journal of Petrology, v. 27(3), p.745-750.

Basu, A., Young, S.W., Suttner, L.J., James, W.C., Mack, G.H. (1975). Re-evaluation of the use of undulatory extinction and polycrystallinity in detrital quartz for provenance interpretation; Journal of Sedimentary Research, v. 45(4), p.873-882.

Bhatia, M.R. (1983). Plate tectonics and geochemical composition of sandstones; The Journal of Geology, v. 91(6), p.611-627.

Bhattacharjee, J., Ghosh, K.K., Bhattacharya, B. (2018). Petrography and geochemistry of sandstone–mudstone from Barakar Formation (early Permian), Raniganj Basin, India: Implications for provenance, weathering and marine depositional conditions during Lower Gondwana sedimentation; Geological Journal, v. 53(3), p.1102-1122.

Biswas, S.K. (1982). Rift basins in western margin of India and their hydrocarbon prospects with special reference to Kutch basin; AAPG Bulletin, v. 66(10), p.1497-1513.

Biswas, S.K. (1987). Regional tectonic framework, structure and evolution of the western marginal basins of India; Tectonophysics, v. 135(4), p.307-327.

Biswas, S. K. (1991). Stratigraphy and sedimentary evolution of the Mesozoic Basin of Kutch, Western India. In: S.K. Tandon, Charu C. Pant and S.M. Casshyap (Eds.), Sedimentary Basins of India, Tectonic Context. Gyanodaya Prakashan, Nainital, p.74-103.

Biswas, S. K. (1993). Geology of Kutch – A compilation of Field Reports (1957-1972), KDM Institute of Petroleum Exploration, 450p.

Bock, B., McLennan, S.M., Hanson, G.N. (1998). Geochemistry and provenance of the middle Ordovician Austin Glen Member (Normanskill formation) and the Taconian orogeny in New England; Sedimentology, v. 45(4), p.635-655.

Boggs Jr, S. (2009). Petrology of Sedimentary Rocks. 2nd ed. Cambridge: Cambridge University Press, 600 p.

Bose, P.K., Ghosh, G., Shome, S., Bardhan, S. (1988). Evidence of superimposition of storm waves on tidal currents in rocks from the Tithonian-Neocomian Umia Member, Kutch, India; Sedimentary Geology, v. 54(4), p.321-329.

Burley, S.D., Kantorowicz, J.D., Waugh, B. (1985). Clastic diagenesis; Geological Society, London, Special Publications, v. 18(1), p.189-226.

Chaudhuri, A., Banerjee, S., Le Pera, E. (2018). Petrography of Middle Jurassic to Early Cretaceous sandstones in the Kutch Basin, western India: Implications on provenance and basin evolution; Journal of Palaeogeography, v. 7(1), p.2.

Cox, R., Lowe, D.R., Cullers, R.L. (1995). The influence of sediment recycling and basement composition on evolution of mudrock chemistry in the southwestern United States; Geochimica et Cosmochimica cta, v. 59(14), p.2919-2940.

Cullers, R.L. (2000). The geochemistry of shales, siltstones and sandstones of Pennsylvanian–Permian age, Colorado, USA: implications for provenance and metamorphic studies; Lithos, v. 51(3), p.181-203.

Desai, B. G. (2016). Ichnological events associated with evolution of Kachchh rift basin, western India. In: S. K. Biswas (Ed.), *Recent studies on the geology of Kachchh;* Special Publication of the Geological Society of India No. 6, p. 114–128.

Desai, B.G. and Biswas, S.K. (2018), Postrift deltaic sedimentation in western Kachchh Basin: Insights from ichnology and sedimentology; Palaeogeography, Palaeoclimatology, Palaeoecology, v. 504, p.104-124.

Dickinson, W.R. and Suczek, C.A. (1979), Plate tectonics and sandstone compositions; Aapg Bulletin, v. 63(12), p.2164-2182.

Dickinson, W.R. (1970). Interpreting detrital modes of graywacke and arkose; Journal of Sedimentary Research, v. 40(2), p.695-707.

Dickinson, W.R. (1985). Interpreting provenance relations from detrital modes of sandstones in Zuffa, G.G. (ed.) Provenance of Arenites; NATO ASI Series C, v. 148. Dordrecht: Springer Netherlands, p. 333–361.

Dickinson, W.R., Beard, L.S., Brakenridge, G.R., Erjavec, J.L., Ferguson, R.C., Inman, K.F., Knepp, R.A., Lindberg, F.A., Ryberg, P.T. (1983). Provenance of North American Phanerozoic sandstones in relation to tectonic setting; Geological Society of America Bulletin, v. 94(2), p.222-235.

Dott, R.H. (1964). Wacke, graywacke and matrix; what approach to immature sandstone classification?; Journal of Sedimentary Research, v. 34(3), p.625-632.

Fedo, C.M., Wayne Nesbitt, H., Young, G.M. (1995). Unravelling the effects of potassium metasomatism in sedimentary rocks and paleosols, with implications for palaeoweathering conditions and provenance; Geology, v. 23(10), p.921-924.

Floyd, P.A. and Leveridge, B.E. (1987), Tectonic environment of the Devonian Gramscatho basin, south Cornwall: framework mode and geochemical evidence from turbiditic sandstones; Journal of the Geological Society, v. 144(4), p.531-542.

Flügel, E. and Munnecke, A. (2010), Microfacies of Carbonate Rocks: Analysis, Interpretation and Application. 2nd ed. Berlin: Springer, p.976.

Fürsich, F.T. and Pandey, D.K. (2003), Sequence stratigraphic significance of sedimentary cycles and shell concentrations in the Upper Jurassic–Lower Cretaceous of Kachchh, western India; Palaeogeography, Palaeoclimatology, Palaeoecology, v. 193(2), p.285-309.

Fürsich, F.T., Pandey, D.K., Callomon, J.H., Jaitly, A.K., Singh, I.B. (2001). Marker beds in the Jurassic of the Kachchh Basin, western India: their depositional environment and sequence-stratigraphic significance; Journal of the Palaeontological Society of India, v. 46(1), p.173-198.

Ghaznavi, A.A., Khan, I., Quasim, M.A., Ahmad, A.H.M. (2018). Provenance, tectonic setting, source weathering and palaeoenvironmental implications of Middle-Upper Jurassic rocks of Ler dome, Kachchh, western India: Inferences from Petrography and Geochemistry; Geochemistry, v. 78(3), p.356-371.

Harnois, L. (1988). The CIW index: a new chemical index of weathering; Sedimentary Geology, v. 55(3), p.319-322.

Hayashi, K.I., Fujisawa, H., Holland, H.D., Ohmoto, H. (1997). Geochemistry of~ 1.9 Ga sedimentary rocks from northeastern Labrador, Canada; Geochimica et Cosmochimica Acta, v. 61(19), p.4115-4137.

Heiri, O., Lotter, A.F., Lemcke, G. (2001). Loss on ignition as a method for estimating organic and carbonate content in sediments: reproducibility and comparability of results; Journal of Paleolimnology, v. 25(1), p.101-110.

Herron, M.M. (1988). Geochemical classification of terrigenous sands and shales from core or log data; Journal of Sedimentary Research, v. 58(5), p.820-829.

Ingersoll, R.V. (1988). Tectonics of sedimentary basins; Geological Society of America Bulletin, v. 100(11), p.1704-1719.

Krishna, J. (2017). Outcrop-Based Sequence Stratigraphic Studies on GTM with Focus on the Kachchh Mesozoic, in Banerjee, S. (ed.) The Indian Mesozoic Chronicle: Sequence Stratigraphic Approach. Singapore: Springer Singapore, p. 145–275.

Lindsey, D.A. (1999). An Evaluation of Alternative Chemical Classifications of Sandstones. U.S. Geological Survey Open-File Report 99–346. Denver, Colorado: p 18.

Mange, M.A. and Maurer, H.F. (1992), Heavy minerals in the study of sediments: their application and limitations. In Heavy Minerals in Colour. Dordrecht: Springer Netherlands, p. 4-10.

Mangtani, P.R. and Joshi, A.V. (2024), Facies analysis and depositional environment of siliciclastic sediments of Mundhan dome, Northwestern Kachchh, Western India; Journal of Sedimentary Environments, v. 9(2), p.197-215.

Mangtani, P.R. and Joshi, A.V. (2025), Provenance and tectonic settings of sandstones of Jhuran Formation (Kimmeridgian to Tithonian); Mundhan dome, Kachchh, Western India; Journal of Sedimentary Environments, v. 10(1), p.23-42.

Manker, J.P. and Griffin, G.M. (1971), Source and mixing of insoluble clay minerals in a shallow water carbonate environment; Florida Bay; Journal of Sedimentary Research, v. 41(1), p.302-306.

McLennan, S.M. and Taylor, S.R. (1991), Sedimentary rocks and crustal evolution: tectonic setting and secular trends; The Journal of Geology, v. 99(1), p.1-21.

McLennan, S.M. (1993). Weathering and global denudation; The Journal of Geology, v. 101(2), p.295-303.

McLennan, S.M., Hemming, S., McDaniel, D.K., Hanson, G.N. (1993). Geochemical approaches to sedimentation, provenance, and tectonics, in Johnsson, M.J. and Basu, A. (eds.) Processes Controlling the Composition of Clastic Sediments; Geological Society of America Special Paper 284, p. 21–40.

Morad, S., Ketzer, J.M., De Ros, L.F. (2000). Spatial and temporal distribution of diagenetic alterations in siliciclastic rocks: implications for mass transfer in sedimentary basins; Sedimentology, v. 47, p.95-120.

Mount, J. (1985). Mixed siliciclastic and carbonate sediments: a proposed first-order textural and compositional classification; Sedimentology, v. 32(3), p.435-442.

Mozherovsky, A.V. and Terekhov, E.P. (1998), Authigenic minerals in early Cretaceous and Paleocene sedimentary rocks of the Yamato Ridge, East Sea; Geosciences Journal, v. 2(3), p.148-159.

Nesbitt, H.W. and Young, G.M. (1982), Early Proterozoic climates and plate motions inferred from major element chemistry of lutites; Nature, v. 299(5885), p.715-717.

Picard, M.D. (1971). Classification of fine-grained sedimentary rocks; Journal of Sedimentary Research, v. 41(1), p.179-195.

Porrenga, D.H. (1967). Glauconite and chamosite as depth indicators in the marine environment; Marine Geology, v. 5(5-6), p.495-501.

Ratcliffe, K.T., Morton, A.C., Ritcey, D.H., Evenchick, C.A. (2007). Whole-rock geochemistry and heavy mineral analysis as petroleum exploration tools in the Bowser and Sustut basins, British Columbia, Canada; Bulletin of Canadian Petroleum Geology, v. 55(4), p.320-336.

Roaldest, E., (1978). Mineralogical and chemical changes during weathering, transportation and sedimentation in different environments with particular references to the distribution of Yttrium and lanthanide elements; Geology. Institute., Univ. of Oslo, Norway.

Roser, B.P. and Korsch, R.J. (1988), Provenance signatures of sandstone-mudstone suites determined using discriminant function analysis of major-element data; Chemical Geology, v. 67(1-2), p.119-139.

Sengupta, S. (2017). Introduction to sedimentology; Second edition, (New Delhi, India: CBS Publishers & Distributor) p. 339.

Sun, L., Gui, H., Chen, S. (2013). Geochemistry of sandstones from the Neoproterozoic Jinshanzhai Formation in northern Anhui Province, China: Provenance, weathering and tectonic setting; Chinese Journal of Geochemistry, v. 32(1), p.95-103.

Suttner, L.J. and Dutta, P.K. (1986), Alluvial sandstone composition and paleoclimate; I, Framework mineralogy; Journal of Sedimentary Research, v. 56(3), p.329-345.

Suttner, L.J., Basu, A., Mack, G.H. (1981). Climate and the origin of quartz arenites; Journal of Sedimentary Research, v. 51(4), p.1235-1246.

Taylor, S.R. and McLennan, S.M. (1985), The Continental Crust: Its Composition and Evolution. Oxford: Blackwell Scientific Publications, p.312.

Tortosa, A., Palomares, M., Arribas, J. (1991). Quartz grain types in Holocene deposits from the Spanish Central System: some problems in provenance analysis; Geological Society, London, Special Publications, v. 57(1), p.47-54.

Verma, S.P. and Armstrong-Altrin, J.S. (2013), New multi-dimensional diagrams for tectonic discrimination of siliciclastic sediments and their application to Precambrian basins; Chemical Geology, v. 355, p.117-133.

Worden, R.H. and Burley, S.D. (2003), Sandstone diagenesis: the evolution of sand to stone; Sandstone Diagenesis: Recent and Ancient, p.1-44.

Worden, R.H. and Morad, S. (eds.) (2003), Clay Mineral Cements in Sandstones. International Association of Sedimentologists Special Publication 34. Oxford: Blackwell Publishing, p.489.

Zwing, A., Matzka, J., Bachtadse, V., Soffel, H.C. (2005). Rock magnetic properties of remagnetized Palaeozoic clastic and carbonate rocks from the NE Rhenish massif, Germany; Geophysical Journal International, v. 160(2), p.477-486.